

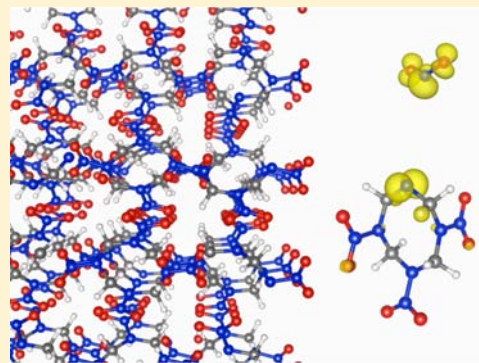
Rapid Materials Degradation Induced by Surfaces and Voids: *Ab Initio* Modeling of β -Octatetramethylene Tetranitramine

Onise Sharia and Maija M. Kuklja*

Department of Materials Science and Engineering, University of Maryland College Park, College Park, Maryland 20742, United States

 Supporting Information

ABSTRACT: A computational strategy based on coupling density functional theory, variational transition state theory, and a microscale materials morphology description unravels details of the defect-induced effect on the surface decomposition of molecular crystals. The technique allows us to resolve the earliest stages of decomposing solids, even for very complex materials and for ultrafast chemical reactions. A comparative analysis of chemical decomposition reactions in HMX with progressively increasing system complexity (an isolated HMX molecule; a perfect single HMX crystal; a defect-containing, porous, and granular HMX crystal) demonstrates that the initiation of the material's degradation can be effectively manipulated by changing the crystal morphology. The activation barriers, reaction constants, and corresponding reaction rates are obtained as a function of molecular environment (a molecule in a vacuum, in an ideal bulk crystal, on a surface or interface, and on a defect in a solid), and decomposition times are predicted. The computational approach can be applied to any other material and system.



1. INTRODUCTION

Surface stability and our ability to understand, predict, and control surface properties of molecular materials and precisely manipulate their chemical compositions are imperative in many research fields such as energy storage and conversion,^{1,2} catalysis,^{3,4} molecular and organic electronics,^{5,6} bio-inspired and bio-mimetic materials,⁷ drug design and materials for chemotherapy,⁸ materials under far-from-equilibrium conditions,⁹ materials synthesis,^{10,11} and sensing and nanotechnology.^{12,13} With most applications requiring very stable surfaces, there are some in which surface degradation (e.g., total or partial decomposition, chemical reactive interactions) defines how efficient the material is for a targeted purpose. For example, surface interactions of tablets/capsules with water and bodily fluids determine the efficiency of medicines in the drug delivery process. Another, even more intriguing example is related to energetic materials in which practically all stages of initiation of combustion and detonation and energy release phenomena involve a great deal of surfaces and interfaces. A fundamental understanding of the microscale details of materials surface behavior (such as the relationship between the structure, chemical composition, and materials functions for targeted applications) does not yet exist despite impressive advances in synthesis and self-assembly that have achieved the enormous level of knowledge and sophistication of molecular constructs during last two decades (see, for example, ref 14).

High energy density molecular materials are known for storing large amounts of the chemical energy that can be rapidly transformed into heat upon external perturbation. Chemical decomposition reactions proceed violently, releasing

huge amounts of thermal energy. Accidental initiation of those reactions may cause a lot of damage and financial loss. Although energetic materials have long been used in a wide range of applications, primarily as fuels, oxidizers, propellants, and explosives, their enormous potential is not fully utilized. Our knowledge and comprehension of the chemistry of the processes underlying initiation of energy release lags substantially behind the need for improving existing and designing new high energy density materials with targeted and well controlled properties. Recent achievements in experimental techniques and quantum-chemical simulations have led to significant progress toward better understanding shock physics phenomena,¹⁵ especially related to the gas phase. Due to its immense complexity, the progress in revealing the behavior of condensed phases has been considerably slower, particularly in aspects related to structural defects and surfaces or interfaces. The interplay between external stimuli, induced materials' response, and complex chemistry makes the study of these materials extremely challenging. Hence, the details of decomposition mechanisms in energetic solids and correlations between the structure, lattice stability, and potential ways that trigger materials' degradation are yet to be established. A detailed understanding of such correlations would open up vast new opportunities in modern life, science, and technology. For instance, new medications, high-precision microsurgeries, synthesis of new materials with targeted superior properties,

Received: May 21, 2012

Published: June 15, 2012

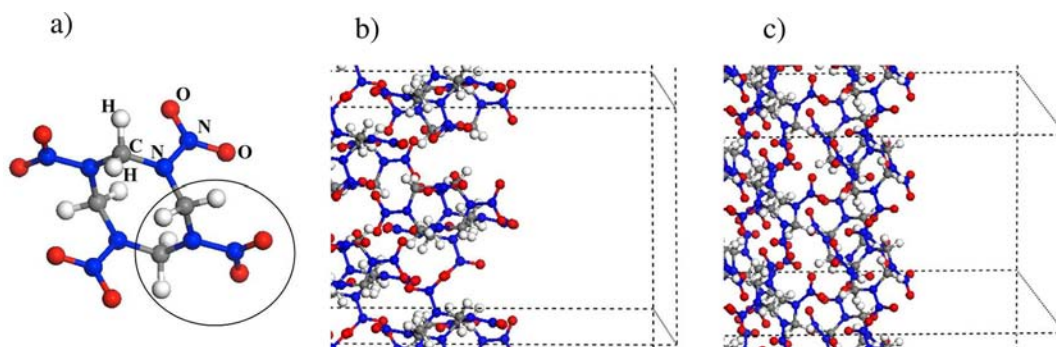


Figure 1. Structures of (a) an HMX molecule, (b) model HMX (100) surface, and (c) model HMX (010) surface. The atoms directly participating in breaking chemical bond reactions and explicitly included in calculations of solid-state molecular vibrations are encircled. The angle between the N–NO₂ bond and the normal of the (100) surface is 77° and of the (010) surface is 38°. The parameters of the supercell slabcut in (100) direction are $a = b = 14.47$ Å, $c = 34.43$ Å, $\alpha = \beta = 90^\circ$, and $\gamma = 104.03^\circ$; those in the (010) direction are $a = 15.164$ Å, $b = 13.4654$ Å, $c = 32.6824$ Å, $\alpha = \beta = 90^\circ$, and $\gamma = 76.704$.

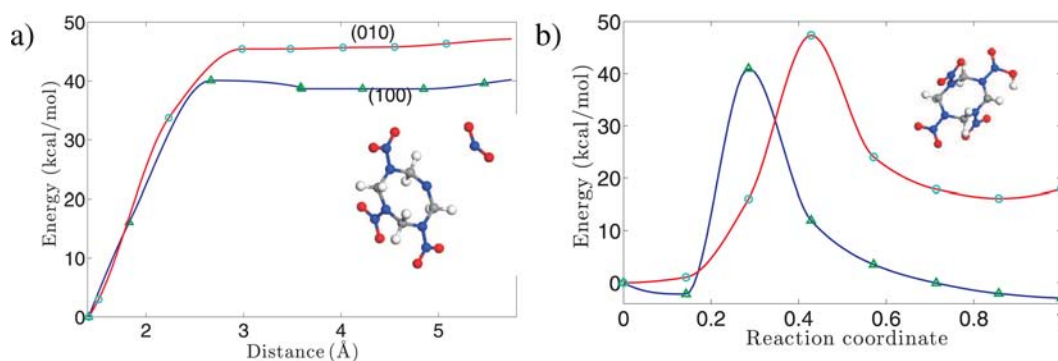


Figure 2. Minimal energy paths for (a) N–NO₂ homolysis and (b) HONO elimination reactions at (100) surface (triangles) and (010) surface (circles). The structure of the corresponding transition state is also shown.

new cutting and drilling microtools, and novel energy and security concepts would become possible.

In this research, aimed at understanding the role internal surfaces play in the decomposition of molecular materials, we present a theoretical and computational strategy that links *ab initio* total energy calculations of defects in a complex molecular material, variational transition state theory, and a microscale description of materials morphology. This strategy, applied to a practical energetic solid, demonstrates that a rapid degradation of molecular materials starts at molecules placed on surface interfaces or molecular defects due to a reduced activation barrier and fast kinetics. We illustrate with β -octahydro-1,3,5,7-tetranitro-1,3,5,7-tetrazocine (β -HMX) how chemical decomposition depends on local molecular surroundings in the perfect and defect containing crystals and whether the particle size in granular materials matters for the initiation process. The organic energetic molecular material HMX was selected for this study for several reasons. The HMX crystal has a complex structure as it is built out of 28-atom molecules. The material is extensively studied. It decomposes with many possible routes, the mechanisms of which are still debated in literature. Any effect of surfaces and defects on its decomposition is yet to be established, and it serves as a good model system for molecular materials. The results of our modeling reveal microscale origins of the surface instability and surface decomposition mechanisms that are difficult or impossible to obtain from experiments alone and provide insights into ways to control fast chemical reactions.

2. DETAILS OF *AB INITIO* CALCULATIONS

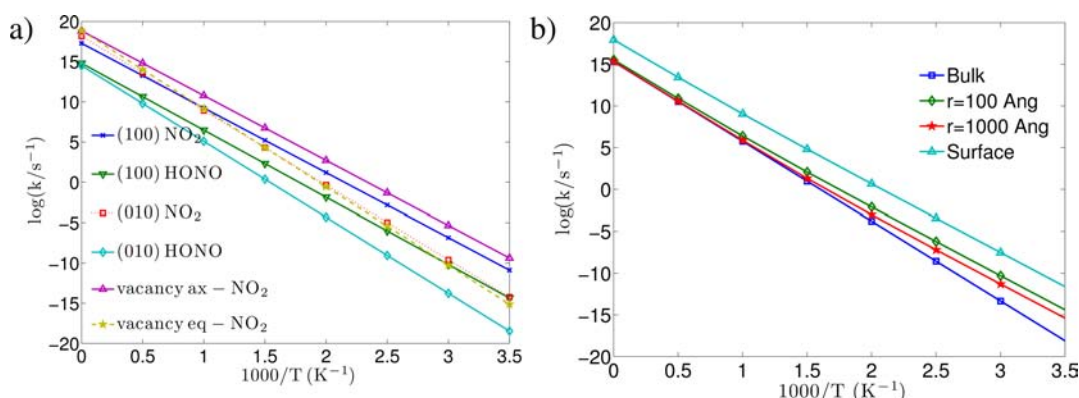
In our calculations, we used a plane wave density functional theory^{16,17} in the generalized gradient approximation (GGA) with Perdew–Burke–Ernzerhof (PBE)¹⁸ functional and Projector Augmented-Wave (PAW)¹⁹ pseudopotentials as implemented in the VASP code.²⁰ The kinetic energy cutoff was set to 600 eV. For the HMX unit cell of $6.7 \times 11.4 \times 8.9$ Å size, we used a $2 \times 2 \times 2$ Monkhorst–Pack²¹ k -point mesh. Atomic positions were relaxed using the conjugate gradient method and quasi-Newtonian method within a force tolerance of 0.025 Å/eV. Minimal energy paths were calculated using the climbing nudged elastic band method²² with six intermediate images. The computationally obtained molecular and crystalline structure of β -HMX is found to be in agreement with the experimental data to within 1–3%.³¹

To explore the surface chemistry, we represent the HMX crystal by using a slab model in which the large 16-molecule supercell was composed of four molecular HMX layers and 10 Å of vacuum in the z direction (Figure 1). The two slabs in our model were chosen to reflect a placement of the equatorial or axial NO₂ groups in the HMX molecule (Figure 1a) at HMX surfaces. The (100) surface cuts the crystal along the direction of the *axial* N–NO₂ bond, and the (010) surface is covered by the *equatorial* NO₂ groups, as illustrated in Figure 1b,c. The full atomic relaxation causes the axial N–NO₂ bond to elongate from 1.373 Å in the bulk to 1.411 Å at the surface and the equatorial N–NO₂ bond to change from 1.391 to 1.413 Å. The different outward relaxations of the NO₂ groups at the (100) and (010) surfaces are also reflected in the different surface energies γ , calculated as

$$\gamma = \frac{1}{2A}(E_{\text{total}} - n_{\text{HMX}}E_{\text{HMX}}) \quad (1)$$

Table 1. Activation Barriers and Reaction Rate Constants for N–NO₂ Homolysis and HONO elimination in an HMX molecule placed in the gas phase, bulk crystal, on a surface or at a vacancy

	gas phase				bulk crystal				surface				vacancy	
	N–NO ₂		HONO		N–NO ₂		HONO		N–NO ₂		HONO		N–NO ₂	
	axi	equ	axi	equ	axi	equ	axi	equ	axi	equ	axi	equ	axi	equ
barrier (kcal/mol)	42.8	44.6	43.4	44.6	47.9	>65	47.9	52.7	40.1	46.3	41.0	48.1	41.0	44.2
ZPE corrected (kcal/mol)	38.1	40.1	39.4	–	43.7	–	45.0	–	37.4	42.2	38.1	43.1	36.5	39.5
rate constant log (k/s ⁻¹)	17.8	18.7	14.2	–	15.1	–	14.3	–	17.3	18.2	14.8	14.5	18.9	18.8

**Figure 3.** (a) Comparison of reaction rates for the N–NO₂ homolysis and HONO elimination for HMX molecules placed on (100) and (010) surfaces and single vacancies. (b) Comparison of N–NO₂ homolysis reaction rates in the presence of internal voids to bulk crystal and pure surface reactions.

where E_{total} is the total energy, A is the surface area, n_{HMX} is the number of HMX molecules in the system, and E_{HMX} is the normalized energy of the bulk HMX per molecule. The obtained energies of the (100) and (010) surfaces are 69.05 and 44.09 mJ/m², respectively; the latter is in agreement with the experimental (010) surface energy of 46 mJ/m².^{23,24}

3. MODELING DECOMPOSITION REACTIONS ON SURFACES AND DEFECTS

Our recent quantum-chemical studies suggested that vacancies,²⁵ dislocations,²⁶ and shear-strain interfaces^{27–29} are imperative in facilitating chemical reactions in energetic molecular crystals. A comparative analysis of the gas-phase HMX³⁰ and solid-state HMX³¹ decomposition processes predicted that *ideal* bulk crystals appear to be more stable and decompose slower than isolated molecules. To apply these findings to practical materials and to relate them to the experiments, the presence of defects and internal surfaces has to be taken into consideration.

The N–NO₂ homolysis was modeled by extending the N–NO₂ bond to 5.5 Å for the (100) surface and to 5.1 Å for the (010) surface. At the indicated distance, NO₂ was dissociated and the system relaxed to a triplet state, similar to its behavior in the gas and crystalline phases.³¹ The N–NO₂ homolysis on the (100) surface requires 40.2 kcal/mol and exhibits a negligible barrier of 1.16 kcal/mol (Figure 2a), and on the (010) surface, it requires 46.3 kcal/mol and proceeds with no barrier. The calculated N–NO₂ homolysis activation energy on either surface is comparable with that in the gas phase (42.8 and 44.6 kcal/mol) and is lower than the activation barrier in a perfect solid HMX bulk (47.9 kcal/mol) (Table 1). This finding is consistent with the conclusion that the activation barrier of a dissociating molecule is defined by intermolecular interactions and therefore is strongly dependent upon the molecular environment, which was shown earlier for a relevant

material RDX.²⁵ It was proposed that the reduction in the bond-breaking energy of surface molecules is caused by the imbalance introduced due to missing intermolecular interactions.²⁵

Further, the HONO isomer formation reaction, which is typically suggested as another possible initiation mechanism in nitro energetics, was modeled by transferring the H atom to the O atom of the nitro group (Figure 2b). The system responds to this perturbation by spontaneous splitting of the entire HONO. Qualitatively, configurations of both the transition state and the final state are similar to those in the gas phase and bulk crystal phase. The energies to form HONO on the (100) and (010) surfaces are 2.94 and 17.92 kcal/mol, respectively, with activation barriers of 40.9 and 47.4 kcal/mol, which are only 1–2 kcal/mol higher than the N–NO₂ homolysis in the corresponding direction. This implies that both mechanisms, the N–NO₂ homolysis and HONO elimination, should contribute as surface initiation reactions in HMX.

Furthermore, a single molecular vacancy in HMX was modeled by removing one HMX molecule from a 16-molecule (2×2×2) supercell; this corresponds to a 6.25% concentration of vacancies in the material. The presence of the vacancy causes a small lattice distortion, in which atoms move about 0.04 Å with the maximum displacement of 0.09 Å, and elongation of the N–NO₂ bond length does not exceed 0.09 Å. The energy of this lattice relaxation is also small, 2.47 kcal/mol. The activation energy required for the axial and equatorial nitro-group homolysis of an HMX molecule placed at the vacancy is 40.0 and 44.2 kcal/mol, respectively (Table 1).

Now, we describe the rate of the HONO elimination reaction with a well-defined transition state and the barrier height E_{B} , by conventional transition state theory.³²

$$k = \frac{k_{\text{B}}T}{h} \frac{Z^{\text{TS}}}{Z^0} e^{-E_{\text{B}}/k_{\text{B}}T} \quad (2)$$

where Z^{TS} and Z^0 are partition functions for the system at the transition point and in the initial configuration, respectively, k_{B} is the Boltzmann constant, h is Planck's constant, and T is the temperature. Calculations of partition functions in a harmonic approximation require the determination of vibrational frequencies at the initial and transition points. To simplify this extremely challenging task, we include vibrations of only those atoms that directly participate in the dissociation reactions (Figure 1a). The numerical error of the pre-exponential factor induced by this approximation is estimated not to exceed 2%.³¹

The kinetics of the N–NO₂ homolysis was described within variational transition state theory.³³ By introducing two simple approximations,³¹ specifically, the NO₂ molecule can be considered as a free rotor and all N–N dissociation directions are equally probable, we derive

$$k = \frac{Z_{\text{rot}}^{\text{NO}_2} Z_{\text{vib}}^{\text{TS}}}{Z_{\text{vib}}^0} \frac{6m_{\text{NO}_2} \pi r^2 (k_{\text{B}} T)^2}{h^3} e^{-E_{\text{B}}/k_{\text{B}} T} \quad (3)$$

where $Z_{\text{rot}}^{\text{NO}_2}$ is a partition function of the NO₂, r is the distance for which the rate becomes minimal ($r = 3 \text{ \AA}$). Figure 3 and Table 1 summarize the results of our calculations. Similarly to the gas phase decomposition,³⁰ there is no big difference in the activation barriers of the HONO elimination and N–NO₂ rupture reactions; however, N–NO₂ homolysis progresses 4–6 orders of magnitude faster. The calculated solid-state reaction barriers for HMX thermal decomposition are within the experimentally reported range of 23–46.6 kcal/mol, with the most reliable data obtained from 33.7 to 46.6 kcal/mol. The calculated reaction constants are in agreement with measured values from 8.5 to 17.0 s⁻¹.³⁴ Most importantly, the N–NO₂ homolysis reactions of the HMX molecule placed at a surface or at a vacancy develop much faster than those in a perfect bulk solid.

Three important conclusions are obtained here. First, the N–NO₂ homolysis, when proceeding in the bulk crystal, requires a fairly high energy (>48 kcal/mol), while the presence of surfaces and vacancies facilitates this decomposition channel by reducing its activation barrier to ~40 kcal/mol, even below the barrier of the isolated molecules (~43 kcal/mol), and making the solid more sensitive than the gas-phase material. Second, the axial nitro group is favored in all cases of probed bond dissociations and suggests that the overall decomposition starts with axial nitro groups. Third, although HONO elimination and nitro group splitting off exhibit quite similar activation barriers, the N–NO₂ fission reaction rate is significantly faster, and therefore it dominates the earliest stages of HMX decomposition.

4. DISCUSSION, INTERPRETATION, AND COMPARISON WITH EXPERIMENT

Now, we will perform a quantitative analysis of the obtained conclusions and link our findings to available experimental data. We find it interesting to explore how/if the surface-enhanced degradation effect is manifested in a decrease of the bulk portion of the material and whether it becomes more pronounced as the reaction progresses. For simplicity and clarity, we will ignore all other reactions besides the N–NO₂ fission and denote the number of surface NO₂ groups (that is the N–NO₂ bonds) as N_{surf} and those in deeper layers of HMX as N_{bulk} . The N–NO₂ decomposition reaction rate may be represented as

$$k = \frac{N_{\text{surf}} k_{\text{surf}} + N_{\text{bulk}} k_{\text{bulk}}}{N} = k_{\text{bulk}} + \frac{N_{\text{surf}}}{N} (k_{\text{surf}} - k_{\text{bulk}}) \quad (4)$$

where $N = 4n_{\text{HMX}}V$ is the total number of NO₂'s in the system. The N_{surf} can be determined using a specific surface area, λ (the total surface area per unit mass), and a surface density of NO₂'s, χ (the number of surface NO₂'s per unit area). For a particle of mass m , the number of surface NO₂ groups is $N_{\text{surf}} = \chi \lambda m$. The reaction rate expressed in terms of the specific surface area is

$$k = k_{\text{bulk}} + \frac{\chi \lambda m}{4n_{\text{HMX}}V} (k_{\text{surf}} - k_{\text{bulk}}) \\ = k_{\text{bulk}} + \frac{\chi \lambda m_{\text{HMX}}}{4} (k_{\text{surf}} - k_{\text{bulk}}) \quad (5)$$

where m_{HMX} is the mass of an HMX molecule. Assuming the voids in HMX have a spherical shape with radius r , the surface area of a single void is $4\pi r^2$, and introducing the void volume fraction x (volume of all voids divided by the total volume of the system), the number of voids is $n = 3Vx/4\pi r^3$. The total surface area of the interior is $3Vx/4r$, and the corresponding specific surface area is $3x/4rm_{\text{HMX}}$. The reaction rate due to internal voids obtained from eq 5 will be

$$k = k_{\text{bulk}} + \frac{3\chi x}{4rm_{\text{HMX}}} (k_{\text{surf}} - k_{\text{bulk}}) \quad (6)$$

where k_{surf} is the aggregate equatorial and axial N–NO₂ homolysis reaction rate, and n_{HMX} is the number of HMX molecules located in a volume unit, $n_{\text{HMX}} = 0.0035 \text{ 1/\AA}^3$. The interpretation of eq 6 is simple yet important: it means that for the given void volume fraction x , the smaller the void size, the higher the reaction rate, or equivalently, the larger the surface area, the faster the decomposition, or (still equivalently) the larger the surface area, the more sensitive the material is to heat. Thus, many small voids (unlike a few large voids) significantly increase the specific surface area and therefore considerably accelerate the degradation of the material.

To relate our equations to available experiments on small internal voids of sizes up to 1000 Å in HMX with a sub-micrometer internal void volume fraction from 0.07 to 2.9%,^{35,36} we simulated HMX with a volume fraction of 1%. Figure 3 displays the reaction rates calculated from eq 6 for the two void radii, 100 and 1000 Å. It is clearly shown that in both cases, the surface reactions are accelerated if compared to ideal bulk HMX, however, 100 Å voids have a substantially more pronounced effect than 1000 Å voids.

Obviously, surface roughness, open pores, cracks, and other imperfections that increase the specific surface area should also make the material decompose faster. This hypothesis is consistent with experimental measurements of defects focused on voids that generally agree that a higher porosity (lower density) greatly increases the ignition sensitivity of energetic materials.^{37–39} In granular materials, the specific surface area increases when a particle size is reduced; hence, the smaller grain size would expect to supply more sensitive material formulations. To prove (or reject) this premise, we estimate from eqs 4 and 5 how much time is required to decompose a bulk layer of an HMX sample as a function of the specific surface area (or grain size) and temperature.

It is established that the N–NO₂ split is the rate-determining reaction in the HMX decomposition, and all of the following reactions have half of this activation energy.⁴⁰ Hence, for

simplicity we assume that once the NO_2 splits off of the surface HMX molecule, the rest of the molecule immediately decomposes, releasing gas products, and at least one bulk HMX molecule becomes a surface molecule. Then, in the lower limit, the number of the surface NO_2 's may be considered constant, $N_{\text{surf}}(t) \geq N_{\text{surf}}(t_0)$, and we can estimate how quickly the bulk $\text{N}-\text{NO}_2$ bonds will be broken in the sample as

$$\frac{\partial N}{\partial t_{\text{bulk}}} = -k_{\text{bulk}}N_{\text{bulk}}(t) - k_{\text{surf}}N_{\text{surf}}(t_0) \quad (7)$$

By solving this equation, we find the total number of freed-up nitro groups as a function of time:

$$N(t) = N_{\text{bulk}}(t_0) \left(1 + \frac{k_{\text{surf}}N_{\text{surf}}(t_0)}{k_{\text{bulk}}N_{\text{bulk}}(t_0)} \right) (1 - e^{-k_{\text{bulk}}t}) \quad (8)$$

The second term in parentheses describes the surface effects. We would like to stress here that although eq 8 is used here to describe $\text{N}-\text{NO}_2$ homolysis in HMX, the formulas (eqs 4–8) are versatile in nature and can be easily generalized to an arbitrary reaction in any molecular material. Table 2 shows two

Table 2. Decomposition Times Required To Dissociate 10% and 2% of $\text{N}-\text{NO}_2$ Bonds in Granular HMX Samples Composed of Coarse ($300 \mu\text{m}$) and Fine ($3 \mu\text{m}$) Particles, Shown at Three Select Temperatures

T (K)	10% fine	10% coarse	2% fine	2% coarse
1400	0.29 ns	0.581 ns	0.057 ns	0.104 ns
1100	14.89 ns	38.92 ns	2.93 ns	7.433 ns
480	942 s	3882 s	197 s	735 s

snapshots of the calculated results: for breaking all $\text{N}-\text{NO}_2$ bonds in 10% and 2% of an HMX sample at three select temperatures. Figure 4 displays the percentage of $\text{N}-\text{NO}_2$

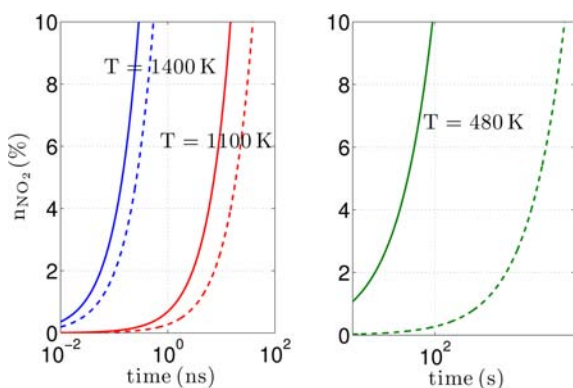


Figure 4. Fraction of split-off NO_2 groups (in %) in a granular HMX sample shown as a function of time for coarse, $300 \mu\text{m}$ particles (dashed lines), and fine, $3 \mu\text{m}$ particles (solid lines).

homolysis reactions as a function of time for two different values of the specific surface area that corresponds to coarse, $300 \mu\text{m}$ (dashed lines), and fine, $3 \mu\text{m}$ (solid lines), HMX particles illustrating that coarse-grain HMX decomposes significantly slower than fine-grain HMX and that this difference becomes considerably smaller with increased temperature. For example, 10% of fine-grain HMX decomposes within 15 ns, while it requires about 40 ns for coarse-grain HMX at 1100 K. At 1400 K, the decomposition of the same amount of the material does not exceed 1 ns. At a lower

temperature of 480 K, 10% of fine-grain HMX takes about 15 min, while coarse-grain HMX will require more than 1 h.

In agreement with VISAR measurements of the detonation wave profiles,⁴¹ the decomposition proceeds visibly faster for fine-grain HMX than for the coarse-grain formulation. In these experiments,⁴¹ the HMX powder contained 2.5 wt % of particles with a size of $400 \mu\text{m}$, 83 wt % of particles $160-400 \mu\text{m}$, 14 wt % of $63-160 \mu\text{m}$ particles, and 0.5% of particles with the size less than $63 \mu\text{m}$, and the average density was from 1.73 to 1.77 g/cm^3 . The fine-grain HMX had a size varying between 1 and $5 \mu\text{m}$, and the average density of grains was $1.858 \pm 0.003 \text{ g/cm}^3$. The sizes of the investigated samples are comparable to the sizes of our model samples, $300 \mu\text{m}$ for coarse-grain HMX and $3 \mu\text{m}$ for fine-grain HMX. We note that the dramatic difference in time needed for low-temperature decomposition becomes orders of magnitude smaller (<0.01 ns) at high temperatures, characteristic of shock and detonation waves. This difference is, in fact, smaller than current experimental techniques can resolve (see Figure 4 and Table 2).

Strictly speaking, a direct comparison of the calculated kinetics to available experiments should be made with caution because the ideal, defect-free arrangement of the materials having only surfaces or voids modeled here cannot be expected from real samples. In addition, thermal decomposition experiments measure only aggregate materials' decomposition and do not distinguish between individual reactions resolved in the present study. Nevertheless, the general trends and obtained conclusions will hold, as the presence of other defects will be likely to amplify the effects revealed.²⁵⁻²⁹ Our calculations demonstrate that the methodology applied here to describe voids, vacancies, internal surfaces, interfaces, and granular materials provides a meaningful tool to quantify and predict the effect of morphology of practical samples on their sensitivity to external thermal perturbation, which is instrumental for the elucidation of molecular stability mechanisms (especially when applied in a combination with high quality experiments).

5. SUMMARY AND CONCLUSIONS

A surface- and vacancy-induced effect on the stability of molecular materials is explored by means of computational modeling of a complex molecular material. The modeling approach that bridged first principles calculations based on density functional theory, variational transition state theory, and variations of morphology of the selected material, is demonstrated to yield dominating decomposition mechanisms including activation barriers, reaction constants, and reaction rates. The activation energy and kinetics of two major decomposition reactions, the $\text{N}-\text{NO}_2$ homolysis and HONO elimination, in HMX are calculated and compared as a function of molecular environment. It is established that an HMX molecule placed on a surface interface or at a vacancy requires a 6–7 kcal/mol lower activation energy for the $\text{N}-\text{NO}_2$ bond-breaking reaction as compared to the bulk crystal and 1–2 kcal/mol lower than an isolated molecule. It was further found that the surface reactions progress orders of magnitude faster than ideal bulk crystal reactions and are comparable to the rate characteristic for the gas phase. The HONO elimination mechanism also exhibits the reduced activation barrier due to the surface effect; however, the pre-exponential factor does not change significantly. Therefore, an increase of the HONO elimination reaction rate is less dramatic than of the $\text{N}-\text{NO}_2$ bond rupture. Overall, we conclude that the $\text{N}-\text{NO}_2$ homolysis

is the dominating reaction in HMX samples containing surfaces, interfaces, voids, or vacancies. Another important finding is that the imperfections, which significantly increase the specific surface area in practical materials, will also lower the activation barriers and accelerate kinetics, resulting in a higher sensitivity to initiation of the material's chemical degradation. This is illustrated for porous crystals and fine particle granular materials. The dramatic difference in decomposition times observed at low temperatures becomes exponentially smaller at high temperature. This research demonstrates that DFT calculations coupled with transition state theory provide a powerful tool for modeling immensely complex physics and chemistry of molecular crystals. This approach proved useful in yielding the details of rapid materials decomposition processes, which are currently not attainable even from advanced experiments alone (e.g., high-resolution fast spectroscopy). A similar computational analysis can be applied to any molecular material and would be especially advantageous when experimental studies are difficult, expensive, or impossible (e.g., materials under extreme conditions or harsh environments, self-assembly, ultrafast chemistry, drug design, chemotherapy, supramolecular and hierarchical materials, multifunctional materials, compound catalysts, and hybrid systems).

■ ASSOCIATED CONTENT

● Supporting Information

Total energies obtained from VASP calculations. This material is available free of charge via the Internet at <http://pubs.acs.org>.

■ AUTHOR INFORMATION

Corresponding Author

mkukla@umd.edu or mkukla@nsf.gov

Notes

The authors declare no competing financial interest.

■ ACKNOWLEDGMENTS

This research is supported in part by ONR (Grant N00014-12-1-0529) and NSF. We used NSF XSEDE resources (Grant DMR-100054) and DOE NERSC resources (Contract DE-AC02-05CH11231). M.M.K. is grateful to the Office of the Director of NSF for support under the IRD program.

■ REFERENCES

- (1) Nazeeruddin, M. K.; Kay, A.; Rodicio, I.; Humphreys, R.; Muller, E.; Liska, P.; Vlachopoulos, N.; Gratzel, M. *J. Am. Chem. Soc.* **1993**, *115*, 6382–6390.
- (2) Somorjai, G. A.; Frei, H.; Park, J. Y. *J. Am. Chem. Soc.* **2009**, *131*, 16589–16605.
- (3) Montoro, C.; Linares, F.; Quartapelle Procopio, E.; Senkovska, I.; Kaskel, S.; Galli, S.; Masciocchi, N.; Barea, E.; Navarro, J. A. R. *J. Am. Chem. Soc.* **2011**, *133*, 11888–11891.
- (4) Xie, X. W.; Li, Y.; Liu, Z. Q.; Haruta, M.; Shen, W. *J. Nature* **2009**, *458*, 746–749.
- (5) Gandhi, D. D.; Lane, M.; Zhou, Y.; Singh, A. P.; Tisch, U.; Eizenberg, M.; Ramanath, G. *Nature* **2007**, *447*, 299–U2.
- (6) O'Regan, B. C.; Durrant, J. R. *Acc. Chem. Res.* **2009**, *42*, 1799–1808.
- (7) Sun, H.; Cao, L.; Lu, L. *Energy Environ. Sci.* **2012**, *5*, 6206–6213.
- (8) Zhang, F.; Braun, G. B.; Pallaoro, A.; Zhang, Y.; Shi, Y.; Cui, D.; Moskovits, M.; Zhao, D.; Stucky, G. D. *Nano Lett.* **2012**, *12*, 61–67.
- (9) Nair, N. N.; Schreiner, E.; Marx, D. *J. Am. Chem. Soc.* **2008**, *130*, 14148–14160.
- (10) Thottampudi, V.; Shreeve, J. M. *J. Am. Chem. Soc.* **2011**, *133*, 19982–19992.

- (11) Manaa, M. R.; Reed Evan, J.; Fried, L. E.; et al. *J. Am. Chem. Soc.* **2009**, *131*, 5483–5487.
- (12) Pramanik, S.; Zhang, C.; Zhang, X.; Emge, T. J.; Li, J. *J. Am. Chem. Soc.* **2011**, *133*, 4153–4155.
- (13) Lee, S. J.; Morrill, A. R.; Moskovits, M. *J. Am. Chem. Soc.* **2006**, *128*, 2200–2201.
- (14) Kaiser, T. E.; Stepanenko, V.; Wuerthner, F. *J. Am. Chem. Soc.* **2009**, *131*, 6719–6732.
- (15) Dlott, D. D. *Annu. Rev. Phys. Chem.* **2011**, *62*, 575.
- (16) Hohenberg, P.; Kohn, W. *Phys. Rev.* **1964**, *136*, B864.
- (17) Kohn, W.; Sham, L. *Phys. Rev. A* **1965**, *140*, 1133.
- (18) Perdew, J. P.; Burke, K.; Ernzerhof, M. *Phys. Rev. Lett.* **1996**, *77*, 3865.
- (19) Blöchl, P. E. *Phys. Rev. B* **1994**, *50*, 953.
- (20) Kresse, G.; Furthmüller, J. *Comput. Mater. Sci.* **1996**, *6*, 15. Kresse, G.; Furthmüller, F. *Phys. Rev. B* **1996**, *54*, 11169. Kresse, G.; Hafner, J. *Phys. Rev. B* **1993**, *47*, RC558.
- (21) Monkhorst, H. J.; Pack, J. D. *Phys. Rev. B* **1976**, *13*, 5188.
- (22) Henkelman, G.; Uberuaga, B. P.; Jónsson, H. *J. Chem. Phys.* **2000**, *113*, 9901.
- (23) Elban, W. L. *J. Mater. Sci.* **1979**, *14*, 1008–1011.
- (24) Yee, R. Y.; Adicoff, A.; Dibble, E. J. Surface properties of HMX crystal. 17th Combustion meetings: papers JANNAF, 1980.
- (25) Kuklja, M. M. *J. Phys. Chem. B* **2001**, *105*, 10159–10162.
- (26) Kuklja, M. M.; Kunz, A. B. *J. Appl. Phys.* **2001**, *89*, 4962–4970. Kuklja, M. M.; Kunz, A. B. *J. Appl. Phys.* **2000**, *87*, 2215–2218.
- (27) Kuklja, M. M.; Rashkeev, S. N.; Zerilli, F. J. *Appl. Phys. Lett.* **2006**, *89*, 071904.
- (28) Kuklja, M. M.; Rashkeev, S. N. *Appl. Phys. Lett.* **2007**, *90*, 151913.
- (29) Kuklja, M. M.; Rashkeev, S. N. *J. Phys. Chem. C* **2009**, *113*, 17–20.
- (30) Sharia, O.; Kuklja, M. M. *J. Phys. Chem. A* **2010**, *114*, 12656–12661.
- (31) Sharia, O.; Kuklja, M. M. *J. Phys. Chem. B* **2011**, *115*, 12677.
- (32) Hanggi, P.; Talkner, P.; Borkovec, M. *Rev. Mod. Phys.* **1990**, *62*, 251–341.
- (33) Garrett, B. C.; Truhlar, D. G. *J. Phys. Chem.* **1979**, *83*, 1052–1079.
- (34) Glascoe, E. A.; Hsu, P. C.; Springer, H. K.; DeHaven, M. R.; Tan, N.; Turner, H. C. *Thermochim. Acta* **2011**, *515*, 58–66.
- (35) Mang, J. T.; Skidmore, C. B.; Hjelm, R. P.; Howe, P. M. *J. Mater. Res.* **2000**, *15*, 1199.
- (36) Peterson, P. D.; Mang, J. T.; Asay, B. W. *J. Appl. Phys.* **2005**, *97*, 093507.
- (37) Gustavsen, R. L.; Sheffield, S. A.; Alcon, R. R. *J. Appl. Phys.* **2006**, *99*, 114907.
- (38) Lecume, S.; Spyckerelle, C.; Sommer, F. *AIP Conf. Proc.* **2004**, *706*, 997.
- (39) Walley, S. M.; Fieldand, J. E.; Greenaway, M. W. *Mater. Sci. Technol.* **2006**, *22*, 402.
- (40) Zhang, S.; Nguyen, H. N.; Truong, T. N. *J. Phys. Chem. A* **2003**, *107*, 2981–2989.
- (41) Kanel, G. I.; Utkin, A. V.; Razorenov, S. V. *Central Eur. J. Energetic Mater.* **2009**, *6*, 15–30.

■ NOTE ADDED AFTER ISSUE PUBLICATION

Octatetramethylene was corrected in the title on August 15, 2012.